Matter

CellPress

Article

A sustainable chitosan-zinc electrolyte for high-rate zinc-metal batteries

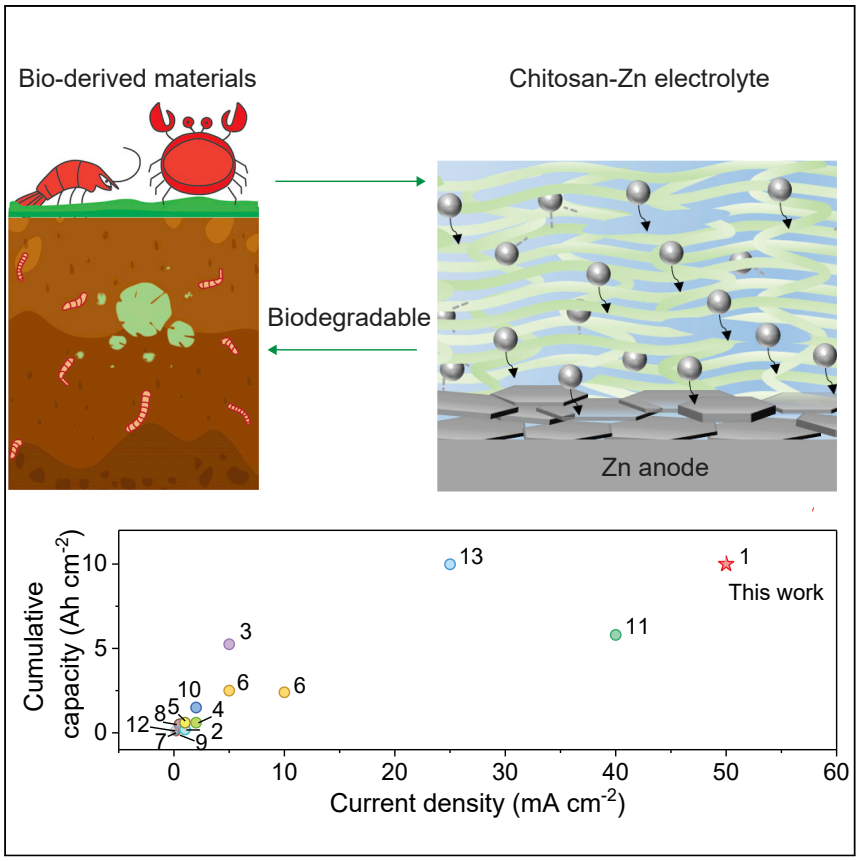

Zn-metal battery is a promising clean energy-storage device, but its application is hindered by uncontrolled Zn deposition in the Zn-metal anode. We find that a biomaterial-derived chitosan-Zn electrolyte enables favorable Zn-platelet deposition due to its high mechanical strength, high Zn^{2+} conductivity, and water bonding capability. The chitosan-Zn electrolyte not only enables high-rate and long-life performance but is also biodegradable, appealing for clean and efficient energy storage.

Demonstrate
Proof-of-concept of performance with intended application/response

Meiling Wu, Ye Zhang, Lin Xu, ..., Shuangshuang Jing, Yan Yao, Liangbing Hu

yyao4@uh.edu (Y.Y.)
binghu@umd.edu (L.H.)

Highlights

A Zn-coordinated chitosan electrolyte is proposed

The chitosan-Zn electrolyte enables a desirable Zn-deposition morphology

Performance of Zn-metal battery with this electrolyte is investigated

Wu et al., Matter 5, 1–15
October 5, 2022
https://doi.org/10.1016/j.matt.2022.07.015

Please cite this article in press as: Wu et al., A sustainable chitosan-zinc electrolyte for high-rate zinc-metal batteries, Matter (2022), https://doi.org/10.1016/j.matt.2022.07.015

Matter

CellPress

Article

A sustainable chitosan-zinc electrolyte for high-rate zinc-metal batteries

Meiling Wu,[1,3] Ye Zhang,[2,3] Lin Xu,[1] Chunpeng Yang,[1] Min Hong,[1] Mingjin Cui,[1] Bryson C. Clifford,[1] Shuaiming He,[1] Shuangshuang Jing,[1] Yan Yao,[2,*] and Liangbing Hu[1,4,*]

SUMMARY

Rechargeable aqueous Zn-metal battery is promising for grid energy storage needs, but its application is limited by issues such as Zn dendrite formation. In this work, we demonstrate a Zn-coordinated chitosan (chitosan-Zn) electrolyte for high-performance Zn-metal batteries. The chitosan-Zn electrolyte exhibits high mechanical strength, Zn^{2+} conductivity, and water bonding capability, which enable a desirable Zn-deposition morphology of parallel hexagonal Zn platelets. Using the chitosan-Zn electrolyte, the Zn anode shows exceptional cycling stability and rate performance, with a high Coulombic efficiency of 99.7% and >1,000 cycles at 50 mA cm^{-2}. The full batteries show excellent high-rate performance (up to 20C, 40 mA cm^{-2}) and long-term cycling stability (>400 cycles at 2C). Furthermore, the chitosan-Zn electrolyte is non-flammable and biodegradable, making the proposed Zn-metal battery appealing in terms of safety and sustainability, demonstrating the promise of sustainable biomaterials for green and efficient energy-storage systems.

INTRODUCTION

To reduce carbon emissions and realize carbon neutrality, it is essential to develop sustainable rechargeable batteries for the storage of renewable energy.[1,2] Aqueous rechargeable batteries, such as Zn-metal batteries, which use a Zn-metal anode and water-based electrolytes, are attractive candidates to fulfill these energy storage demands due to their inherent safety, fast charging/discharging capability, environmental friendliness, wide material availability, and low cost.[3,4] However, rechargeable Zn-metal batteries have yet to be commercialized, largely because of problems associated with the Zn-metal anode, including undesired Zn dendrite formation, corrosion, and hydrogen generation during the Zn plating/stripping process,[5,6] all of which can cause low cycling reversibility and ultimately battery failure.

These issues mainly stem from the unregulated Zn-deposition morphology at high current densities as well as the high free-water content in conventional aqueous electrolytes, which reacts with the Zn-metal during electrochemical cycling.[7–10] The aqueous electrolyte induced the surface passivated reactions on Zn surface, which lead to inhomogeneous Zn deposition that cause possible dendrite penetration through the separator and low cycling reversibility.[11–13] To address these challenges, extensive efforts have been devoted to modifying the electrolyte, including the use of high-salt-concentration "water-in-salt" electrolytes,[14–16] various additives to aqueous electrolytes (such as ethylene glycol as a water blocker),[17,18] or organic electrolytes.[19,20] However, these strategies sacrifice the intrinsic high conductivity of

PROGRESS AND POTENTIAL

Rechargeable aqueous Zn-metal batteries have a strong potential to fulfill the needs of large-scale grid energy storage. However, the use of aqueous electrolytes has created various challenges, such as inhomogeneous Zn dendrite formation. Although many efforts have been devoted to investigating Zn-metal batteries, their rate performance and cycling life are still limited. Here, we demonstrate a Zn-coordinated chitosan as an excellent Zn battery electrolyte with a high Zn^{2+} conductivity, high mechanical strength, and favorable Zn-deposition morphology, enabling Zn-metal batteries with outstandingly high-rate performance and long-term cycling stability. In addition, the biodegradable property of chitosan-based electrolytes makes it possible to fabricate biodegradable and sustainable Zn batteries. The biopolymeric chitosan-based electrolyte and its design strategy will advance the development of high-performance and sustainable biopolymer-based electrolytes for green energy storage.

Please cite this article in press as: Wu et al., A sustainable chitosan-zinc electrolyte for high-rate zinc-metal batteries, Matter (2022), https://doi.org/10.1016/j.matt.2022.07.015

aqueous electrolytes and/or compromise the safety of the Zn-metal battery.[21] There are reports of hydrogel electrolytes that show promise at inhibiting Zn dendrites, as the nanochannels and polar groups of the hydrogel can control the free-water content and enhance the uniformity of the current distribution.[9,22–24] However, current hydrogel electrolytes do not meet the high mechanical strength, high rate capability, and long-term cycling stability needed for high-performance Zn-metal batteries.[1,25]

In this work, we demonstrate a biopolymeric chitosan-Zn gel electrolyte for high-rate and long-life Zn-metal batteries that features a strong combination of high ionic conductivity, mechanical strength, and sustainability while also enabling a desirable deposition morphology of parallel hexagonal Zn platelets (rather than Zn dendrites) on the anode surface. Chitosan is an eco-friendly and biodegradable biopolymer derived from naturally abundant chitin, which is widely available in crustacean shells.[26] The chitosan molecules contain rich hydroxyl and amine groups that can form hydrogen bonds with water to reduce the content of free water in the chitosan-Zn gel electrolyte. We fabricate this gel electrolyte by first coordinating the chitosan biopolymer with Zn^{2+} in a Zn^{2+}-saturated NaOH solution and then squeezing out excess water by compressing the material, forming a densified chitosan-Zn membrane (Figure 1A). Prior to densification, the porous chitosan-Zn contains a high amount of water, resulting in unregulated Zn deposition that readily forms mossy dendrites (Figure 1B). However, by tailoring the water content through densification, which confines the aqueous electrolyte to nanoscale micropores, we can achieve a high Zn^{2+} ionic conductivity (72 mS cm^{-1}) in addition to the electrodeposition of Zn as parallel platelets on the Zn anode at high current densities (5–50 mA cm^{-2}). This morphology helps to prevent interfacial side reactions and dendrite penetration (Figure 1C). As a result, the Zn anode with the densified chitosan-Zn electrolyte displays excellent reversibility with a high Coulombic efficiency of 99.7% and long cycle life of >1,000 cycles at 50 mA cm^{-2}. Using the chitosan-Zn electrolyte and a poly(benzoquinonyl sulfide) (PBQS) organic cathode with a high mass loading (10 mg cm^{-2}), we demonstrate Zn-metal full cells with a high areal capacity (2.3 mAh cm^{-2}) and good cycling stability (2 C, 4 mA cm^{-2} for >400 cycles). Furthermore, the chitosan-Zn electrolyte is non-flammable and biodegradable, allowing for the fabrication of safe and eco-friendly Zn-metal batteries when paired with the biodegradable organic cathode and recyclable Zn-metal anode. These advantages of the chitosan-Zn electrolyte not only enable high-rate and durable Zn-metal batteries but also suggest the potential of natural biopolymers for sustainable and green energy-storage applications.

RESULTS AND DISCUSSION

Material fabrication and characterization

We prepared the chitosan-Zn membrane using a two-step process (Figure S1A; see experimental procedures for more details). First, we cast a chitosan solution (4 wt % chitosan in 4 wt % acetic acid aqueous solution) on a polyethylene terephthalate (PET) support and then immediately immersed it into a Zn^{2+}-saturated NaOH solution (0.6 wt % Zn^{2+}) to obtain the chitosan-Zn membrane. Next, we rinsed the membrane with water until the pH of the washing solution was 7, followed by mechanically pressing at a pressure of ~5 MPa to produce the final densified chitosan-Zn membrane. The chitosan-Zn membrane without pressing (Figure 2A) shows a hierarchically porous structure, with large pores of up to 5 μm in diameter (Figures 2B and 2C). These pores are generated as a result of phase separation of the polymeric chitosan that is induced by the solvent-nonsolvent exchange process.[27] Compressing

[1]Department of Materials Science and Engineering, University of Maryland, College Park, MD 20742, USA

[2]Department of Electrical and Computer Engineering and Texas Center for Superconductivity at the University of Houston (TcSUH), University of Houston, Houston, TX 77204, USA

[3]These authors contributed equally

[4]Lead contact

*Correspondence: yyao4@uh.edu (Y.Y.), binghu@umd.edu (L.H.)

https://doi.org/10.1016/j.matt.2022.07.015

Please cite this article in press as: Wu et al., A sustainable chitosan-zinc electrolyte for high-rate zinc-metal batteries, Matter (2022), https://doi.org/10.1016/j.matt.2022.07.015

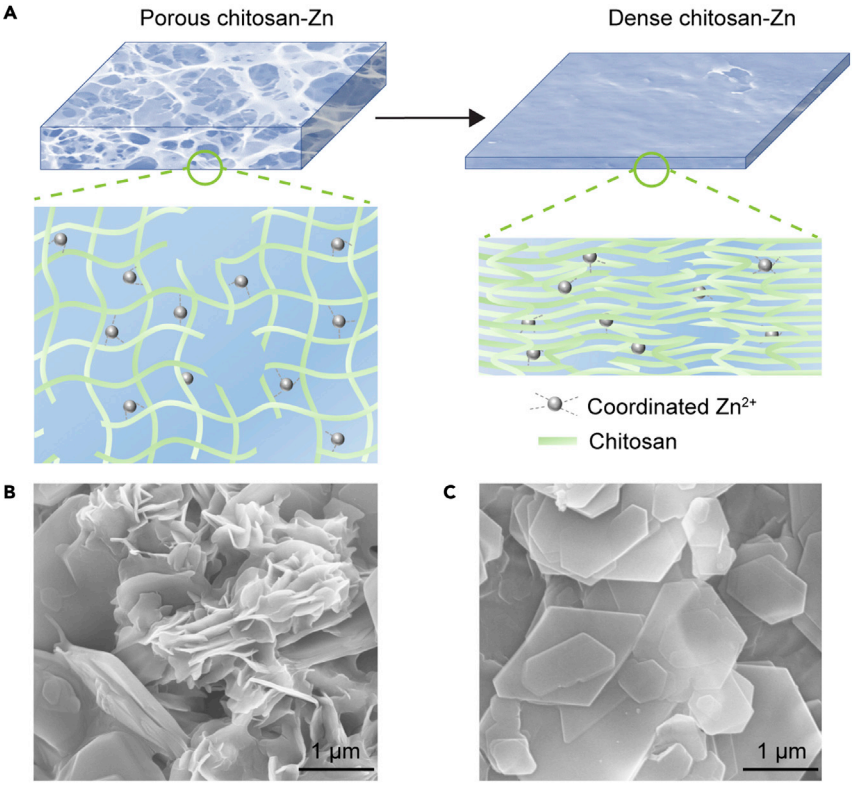

Figure 1. Chitosan-Zn electrolyte and the corresponding Zn plating morphologies in Zn-metal batteries

(A) Schematic comparison of the porous chitosan-Zn with flooded aqueous electrolyte and densified chitosan-Zn electrolyte. The chitosan polymer chains are coordinated with Zn^{2+} to form the porous chitosan-Zn membrane (left). The porous chitosan-Zn is then compressed to make the dense chitosan-Zn electrolyte (right).

(B and C) Scanning electron microscopy (SEM) images of electrochemically deposited Zn-metal anodes that were cycled using (B) the porous chitosan-Zn electrolyte, which results in randomly deposited Zn dendrites, and (C) the dense chitosan-Zn electrolyte, which enables the deposition of parallel-stacked Zn plates.

the porous chitosan-Zn membrane produces a flexible chitosan-Zn membrane (Figure 2D). Top-view and cross-sectional scanning electron microscopy (SEM) images of the pressed chitosan-Zn membrane reveal no obvious pores at the micrometer scale, showing that the membrane is densified compared with the porous starting material (Figures 2E–2F and S1B). Additionally, energy-dispersive X-ray spectroscopy (EDS) elemental mapping of the chitosan-Zn membrane (Figure S1C) confirms that the Zn^{2+} ions are homogeneously dispersed throughout the chitosan. As a control sample, a pure chitosan membrane was prepared by a similar procedure, only replacing the immersion solution with just 20 wt % NaOH (i.e., no Zn^{2+} ions), producing a structure similar to the chitosan-Zn membrane (Figure S2).

We performed X-ray photoelectron spectroscopy (XPS) and Fourier-transform infrared (FTIR) spectroscopy to investigate the chemical valences and bonding states in the densified chitosan-Zn and chitosan membranes. The Zn 2p peaks in the XPS spectrum of the chitosan-Zn membrane clearly show the presence of Zn^{2+} (Figure S3A). In the N 1s XPS spectrum, both samples display a peak at 400 eV due to the $–NH_2$ groups of chitosan. However, the chitosan-Zn membrane also features a peak at 401.8 eV in the N 1s spectrum, which is attributed to the $–N\cdots Zn^{2+}$

Please cite this article in press as: Wu et al., A sustainable chitosan-zinc electrolyte for high-rate zinc-metal batteries, Matter (2022), https://doi.org/10.1016/j.matt.2022.07.015

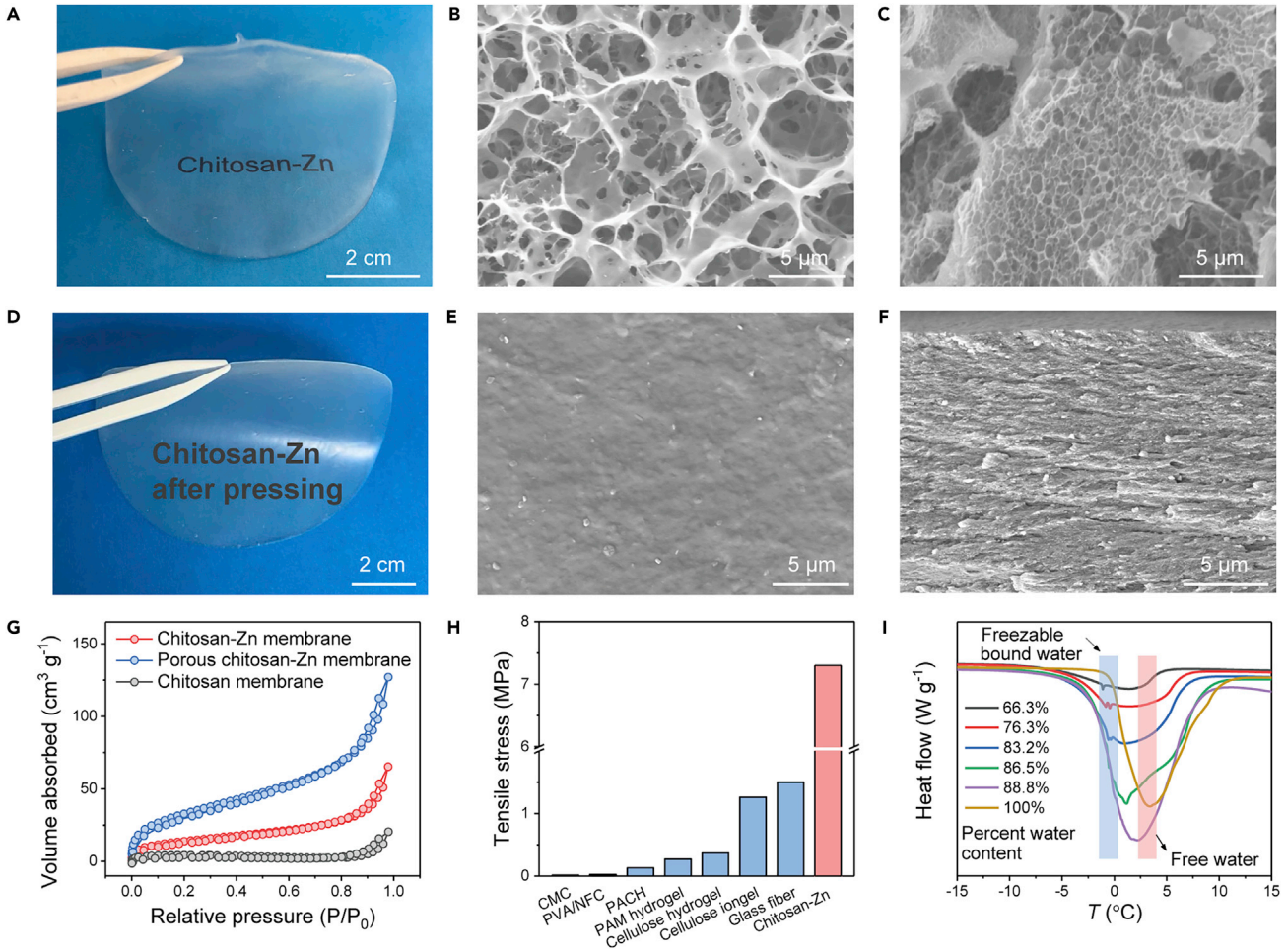

Figure 2. Morphology and characterization of the chitosan-Zn membranes

(A) Photo of the porous chitosan-Zn membrane.

(B and C) SEM images of the (B) surface and (C) cross-sectional morphology of the porous chitosan-Zn membrane.

(D) Photo of the chitosan-Zn membrane after pressing.

(E and F) SEM images of the (E) surface and (F) cross-sectional morphology of the chitosan-Zn membrane after pressing.

(G) The N_2 isotherm adsorption/desorption curves of the chitosan-Zn, porous chitosan-Zn, and chitosan membranes.

(H) Comparison of the ultimate tensile stress of the chitosan-Zn membrane with other reported membranes.[23,29–33]

(I) DSC curves of chitosan-Zn membranes with different percentages of water content. Pure water, noted as 100%, was tested as a reference.

coordination bond,[28] indicating that the $–NH_2$ groups are partially coordinated with Zn^{2+} ions (Figure S3B). Additionally, the FTIR adsorption of the $–NH_2$ bending vibration shifts from 1,590 cm^{-1} in chitosan to 1,523 cm^{-1} in the chitosan-Zn membrane, further suggesting the coordination between $–NH_2$ and Zn^{2+} (Figure S3C). Meanwhile, the broad adsorption of the C–O bond in the chitosan-Zn sample shifts from 1,027 to 1,065 cm^{-1}, indicating that the –OH groups on chitosan are coordinated with Zn^{2+} as well (Figure S3C). These results suggest the Zn^{2+} ions coordinate with both the $–NH_2$ and –OH groups of the chitosan in the chitosan-Zn membrane, which could cross-link the polymeric chitosan chains.

We measured the N_2 adsorption/desorption isotherms of the densified chitosan, porous chitosan-Zn, and densified chitosan-Zn membranes to compare their surface area (Figures 2G and S4). The porous chitosan-Zn membrane has the largest Brunauer-Emmett-Teller (BET) surface area (117.8 $m^2\ g^{-1}$) and pore volume, mainly

Please cite this article in press as: Wu et al., A sustainable chitosan-zinc electrolyte for high-rate zinc-metal batteries, Matter (2022), https://doi.org/10.1016/j.matt.2022.07.015

featuring macropores (Figure 2B). In contrast, pressing the chitosan-Zn membrane eliminates most macroscale pores (Figure 2E), resulting in a moderate BET surface area (17.8 m^2 g^{-1}). Additionally, the densified chitosan-Zn membrane features a higher BET surface area compared with the pure densified chitosan membrane, mainly due to the presence of micropores and mesopores, which are formed due to the coordination between the chitosan and Zn^{2+}. The densification and Zn-coordination process also increases the mechanical strength of the densified chitosan-Zn membrane (Figure S5), which features a high tensile strength of 7.4 MPa—much higher than that of other Zn^{2+} electrolytes (e.g., cellulose hydrogel,[23] CMC membrane[29]) as well as the glass-fiber separator that is commonly used in Zn-metal batteries (Figure 2H). Such an improvement in mechanical strength should be beneficial for suppressing dendrite penetration through the chitosan-Zn electrolyte.

While water plays an important role in the ion conduction of electrolytes, excess water also induces side reactions and dendrite formation on the Zn-metal anode.[9,10] Thus, we evaluated the water-absorption ability and water content of the chitosan-Zn membrane. Different water contents (66.3–88.8 wt %) can be achieved by soaking chitosan-Zn membranes in water or through evaporation. We hypothesized that due to the hydrophilic hydroxyl and amine groups of chitosan, the chitosan-Zn would be able to confine water molecules via hydrogen bonding, thus reducing the ratio of free water in the membrane. Indeed, differential scanning calorimetry (DSC) showed that the chitosan-Zn membranes with different water contents featured both bound water and free water (Figure 2I). The water bonding capability of the chitosan-Zn membrane may help reduce side reactions of the aqueous electrolyte with the Zn-metal anode, which could improve the battery performance.

Conductivity and Zn electrodeposition behavior

We found the chitosan-Zn membrane serves as an excellent Zn^{2+} electrolyte with a high Zn^{2+} ionic conductivity and advantageous Zn plating behavior. The chitosan-Zn electrolytes were obtained by immersing the porous chitosan-Zn membranes in 2 M $ZnSO_4$ aqueous solution, followed by the densifying procedure. The excellent wettability of the chitosan-Zn membrane toward $ZnSO_4$ aqueous solution (Figure S6) facilitates the sufficient adsorption of $ZnSO_4$ into the porous chitosan-Zn membrane and the successful fabrication of high performance of chitosan-Zn electrolyte. By evaporation or through soaking in water, chitosan-Zn electrolytes with different water contents (15%–72%) were prepared. We tested the ionic conductivities of chitosan-Zn electrolytes with different water contents (Figures 3A and S7) and compared them with the 2 M $ZnSO_4$ aqueous electrolyte with a glass-fiber separator (Figure 3B) by electrochemical impedance spectroscopy (EIS). The chitosan-Zn electrolyte with a low water content of 15% showed a low conductivity of 0.03 mS cm^{-1}, which would prevent high-rate Zn cycling. By increasing the water content to 57%, a high conductivity of 71.8 mS cm^{-1} in chitosan-Zn electrolyte was achieved, close to that of the aqueous Zn^{2+}-electrolyte solution and a standout among previously reported Zn^{2+} electrolytes (Table S1). Further increasing the water content to over 57% does not significantly enhance the ionic conductivity. If the porous chitosan-Zn membrane is not immersed in $ZnSO_4$ aqueous solution, a much lower conductivity of 1.22×10^{-5} S cm^{-1} is received (Figure S8), which demonstrates that Zn^{2+} from $ZnSO_4$ in chitosan-Zn electrolyte is mobile and responsible for the Zn^{2+} transport. In contrast, coordinated Zn^{2+} in chitosan-Zn membrane is almost not mobile but provides strong mechanical strength and porous nanostructure.

We applied a galvanostatic plating/stripping method to investigate the Zn plating behavior in Zn||Zn cells using chitosan-Zn electrolytes with different water contents

Please cite this article in press as: Wu et al., A sustainable chitosan-zinc electrolyte for high-rate zinc-metal batteries, Matter (2022), https://doi.org/10.1016/j.matt.2022.07.015

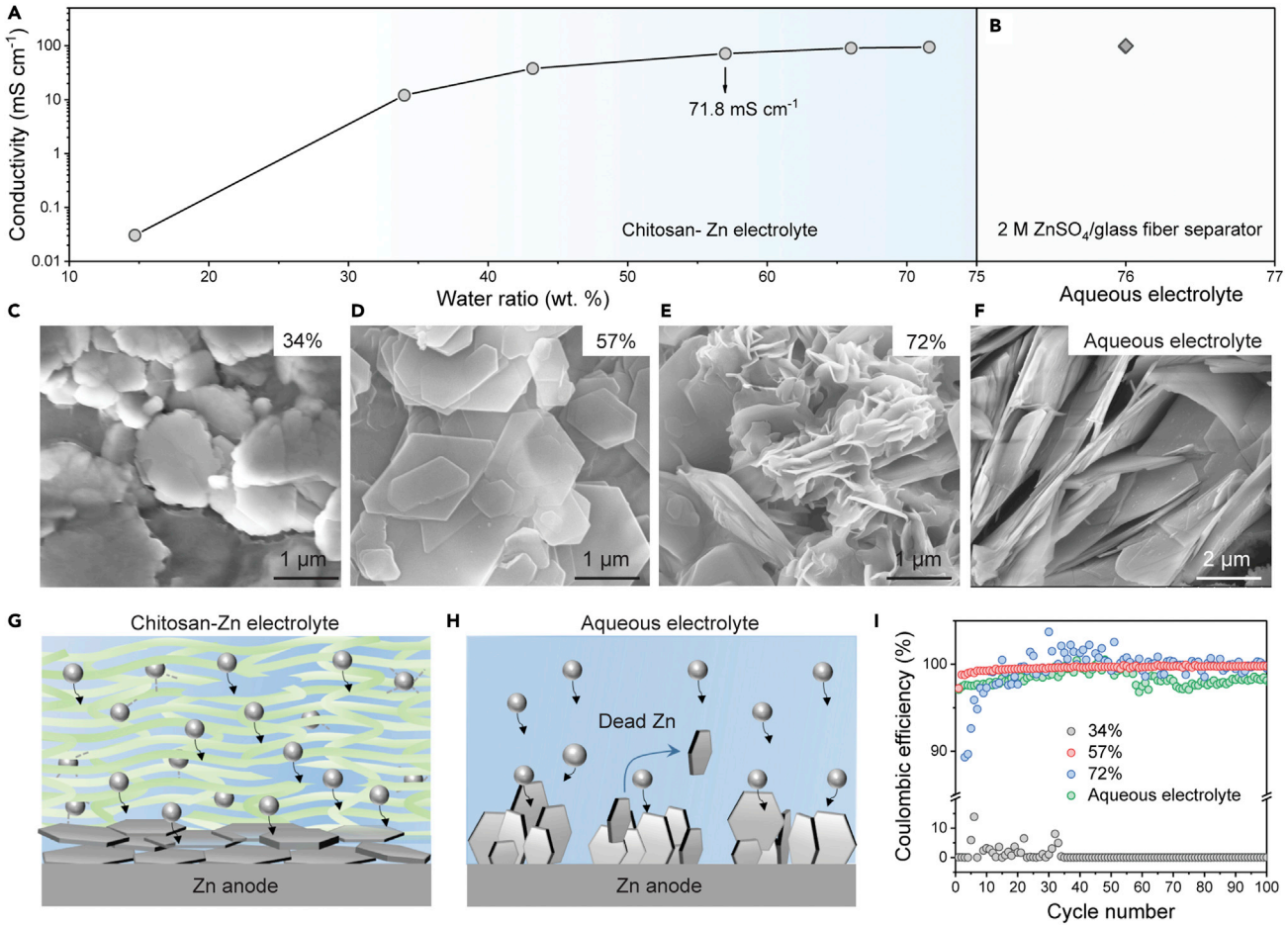

Figure 3. Zn plating behavior

(A) The conductivity of the chitosan-Zn electrolytes with different water contents (15%–72%).

(B) The conductivity of the aqueous electrolyte (2 M $ZnSO_4$, featuring 76% water content and using a glass-fiber separator).

(C–F) Morphology of the Zn plating on the Zn anode after cycling at 20 mA cm^{-2} and 4 mAh cm^{-2} for 50 cycles in Zn||Zn cells with different chitosan-Zn electrolytes containing water contents of (C) 34%, (D) 57%, and (E) 72%, as well as using the (F) 2 M $ZnSO_4$ aqueous electrolyte with a glass-fiber separator.

(G and H) Schematic diagrams of Zn plating on the Zn anode using different electrolytes, including (G) chitosan-Zn and (H) aqueous electrolyte.

(I) The Coulombic efficiency of Zn||Cu cells using different chitosan-Zn electrolytes with varied water contents, as well as 2 M $ZnSO_4$ aqueous electrolyte, at 5 mA cm^{-2} and 5 mAh cm^{-2}.

(34%, 57%, and 72%) and compared them with the pure aqueous electrolyte of 2 M $ZnSO_4$. After cycling at 20 mA cm^{-2} and 4 mAh cm^{-2} for 50 cycles, we used SEM to observe the Zn plating morphology on the Zn anodes (Figures 3C–3F and S9A). The chitosan-Zn electrolyte with 34% water content had a large plating overpotential compared with the 57%-water-content sample (Figure S10) and can only deposit limited Zn (Figure 3C). When using the chitosan-Zn electrolyte with 43% and 57% water contents, the plated Zn forms hexagonal Zn platelets with an orientation parallel to the Zn electrode surface (Figures S9B–S9D and 3D). Transmission electron microscopy (TEM) images of the plating Zn using the 57%-water-content electrolyte show that the hexagonal Zn platelets are composed of small hexagonal Zn domains, with (0002) planes in the in-plane direction and (−1010) planes in the through-plane direction (Figure S11). We also found that the size of the Zn hexagonal platelets grows with the cycle number, from ~200 nm (20 cycles; Figure S12) to >1 μm (50 cycles; Figure 3D), which reduces the surface area of the Zn anode and suppresses the

Please cite this article in press as: Wu et al., A sustainable chitosan-zinc electrolyte for high-rate zinc-metal batteries, Matter (2022), https://doi.org/10.1016/j.matt.2022.07.015

interfacial side reactions. While the 66%- and 72%-water-content chitosan-Zn electrolytes and aqueous electrolyte (2 M $ZnSO_4$) provide slightly higher conductivities (90, 94, and 99 mS cm^{-1}, respectively), the higher amount of free water in these electrolytes leads to unfavorable Zn plating morphologies. The high-water-content chitosan-Zn electrolytes display a mossy Zn plating morphology (Figures 3E, S9E, and S9F), and using the aqueous electrolyte with a glass-fiber separator results in Zn platelets perpendicular to the Zn electrode surface (Figure 3F). The mossy Zn dendrites could cause increased interfacial side reactions with the electrolyte, and their perpendicularly oriented morphologies could lead to dendritic short circuiting. Therefore, the chitosan-Zn electrolyte with a water content of just 57% is more advantageous, as it displays both high conductivity and a superior Zn plating morphology.

The deposition of hexagonal Zn platelet is because the (0002) plane of Zn has a lower surface energy (0.33 J m^{-2}) than other planes (e.g., 0.53 J m^{-2} of the (−1010) plane), which causes the preferential crystal growth of Zn in the (0002) plane, forming hexagonal platelets.[34] The chitosan-Zn electrolyte enables fast and uniform Zn^{2+} conduction while also limiting ion flux perpendicular to Zn anode surface, forming parallel Zn platelets compactly stacked on the anode (Figure 3G). Such a deposition morphology can reduce the electrolyte-Zn interface area and interfacial side reactions, preventing the formation of inactive dead Zn and also reducing the possibility of dendrite penetration through the separator, all of which improved the Zn anode cycling reversibility and lifespan. In contrast, while the aqueous electrolyte also has a high Zn^{2+} ionic conductivity, the Zn^{2+} supply is ubiquitous and from all directions. Thus, in the liquid electrolyte, Zn^{2+} ions diffuse via the shortest path, and the plated Zn-metal tends to form platelets oriented perpendicular to the anode surface (Figure 3H),[35,36] which is adverse to the anode reversibility and stability.

The Zn cycling reversibility of the chitosan-Zn electrolyte is evidenced by the Coulombic efficiency of the Zn-metal anode, which we investigated by cycling Zn||chitosan-Zn||Cu cells at 5 mA cm^{-2} with a capacity of 5 mAh cm^{-2} (Figure 3I). Using the chitosan-Zn electrolyte with 57% water content, the cell shows a Coulombic efficiency of ~99.5% after 100 cycles, indicating excellent Zn plating/stripping reversibility. In contrast, the Coulombic efficiency of the Zn anode with the aqueous $ZnSO_4$ electrolyte is not stable, fluctuating in the range of 96.8%–99.6%, due to inhomogeneous Zn deposition (Figure S13A). The chitosan-Zn electrolyte with a lower water content of 34% showed a low Coulombic efficiency of <2% and the chitosan-Zn electrolyte with more water (72%) showed a Coulombic efficiency of <99% in the first ten cycles but then significantly fluctuated over subsequent cycles, showing a poor reversibility (Figure 3I). We attribute the high and stable Coulombic efficiency of the 57%-water-content chitosan-Zn electrolyte to the material's superior Zn plating morphology, in which the parallel Zn platelets deposited on the Zn anode help suppress dendrite formation and penetration through the chitosan-Zn membrane (Figure S13B), allowing for stable and reversible Zn plating/stripping.

Electrochemical performance

We further tested the Coulombic efficiency at high-current-density and high-capacity conditions in Zn||Cu cells to evaluate the performance of the Zn anode made with the 57%-water-content chitosan-Zn electrolyte (which was used in all following experiments unless otherwise indicated). The Zn||Cu cells show a high Coulombic efficiency of 99.3% for 1,300 cycles at 5 mA cm^{-2} with a capacity of 1 mAh cm^{-2} and 99.8% at 5 mA cm^{-2} with a capacity of 5 mAh cm^{-2} (FigureS S14A and S14B). We further cycled the cells at 10 mA cm^{-2} with a capacity of 2 mAh cm^{-2}, which showed

Please cite this article in press as: Wu et al., A sustainable chitosan-zinc electrolyte for high-rate zinc-metal batteries, Matter (2022), https://doi.org/10.1016/j.matt.2022.07.015

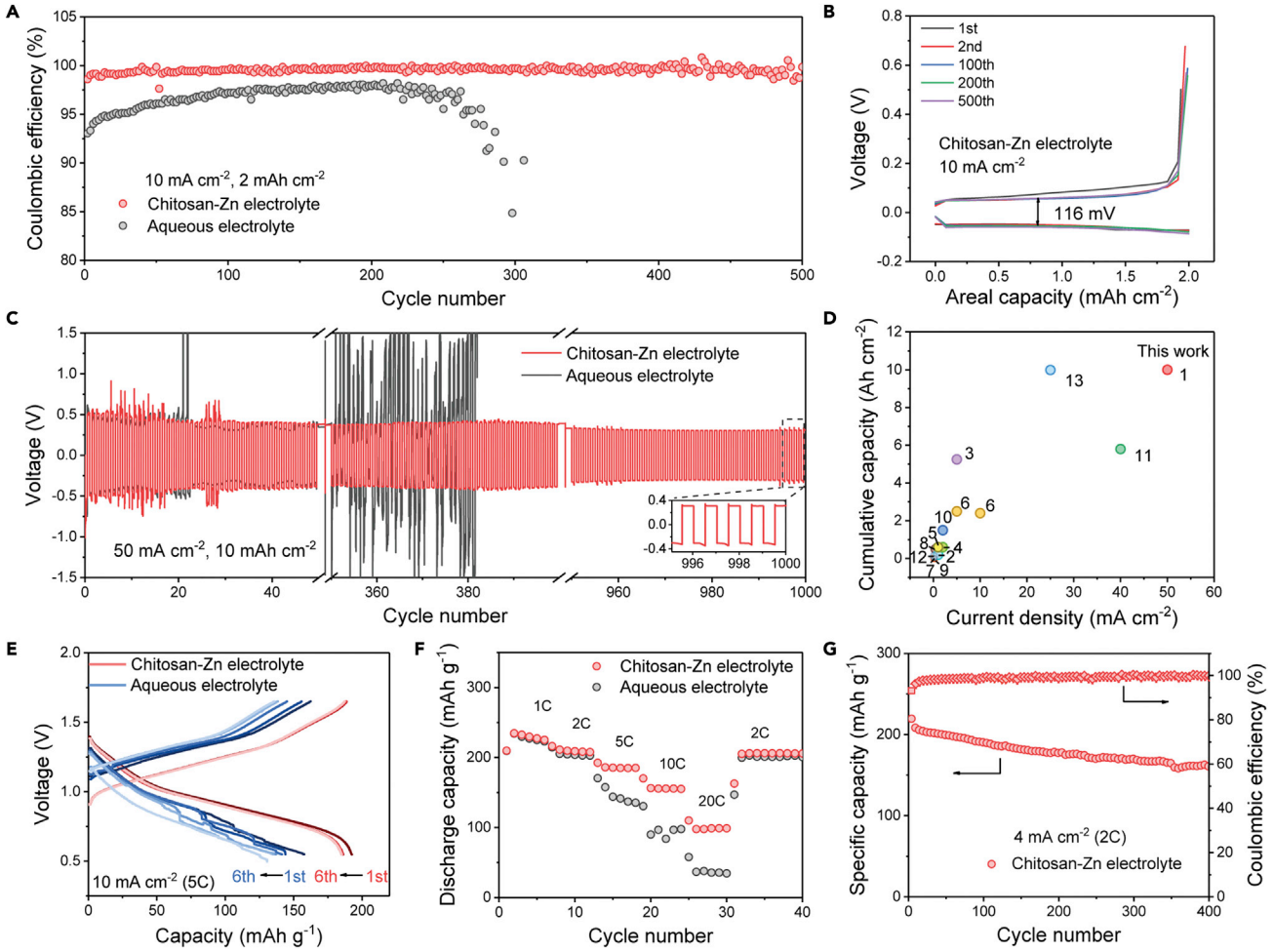

Figure 4. Electrochemical performance of Zn plating/stripping using chitosan-Zn and aqueous electrolytes

(A and B) The Zn plating/stripping Coulombic efficiency on a Cu electrode cycled with chitosan-Zn and aqueous electrolytes at 10 mA cm^{-2} and 2 mAh cm^{-2} (A) and the corresponding Zn plating/stripping voltage profiles on a Cu electrode cycled with chitosan-Zn electrolyte (B).

(C) Galvanostatic Zn plating/stripping in a Zn||Zn symmetric cell cycled with chitosan-Zn and aqueous electrolytes at 50 mA cm^{-2} and 10 mAh cm^{-2}.

(D) Performance comparison of the Zn||Zn symmetric cell in terms of the current density and cumulative capacity cycled using the chitosan-Zn electrolyte and other reported electrolytes.[15–18,51–58]

(E) Galvanostatic charge-discharge potential profiles of the Zn||PBQS cell using chitosan-Zn electrolyte and aqueous electrolyte at 5C rates. The PBQS loading was 10 mg cm^{-2}.

(F) Rate performance comparison of the Zn||PBQS battery using the chitosan-Zn and aqueous electrolyte with a rate ranging from 1 to 20C.

(G) Cycling performance of the Zn||PBQS cell using the chitosan-Zn electrolyte at 2C with a PBQS loading of 10 mg cm^{-2}.

a high Coulombic efficiency of 99.7% for 500 cycles (Figure 4A). In contrast, using the aqueous $ZnSO_4$ electrolyte or the porous chitosan-Zn electrolyte (without the densifying step and therefore containing more water), the Coulombic efficiencies are low and not stable (Figures 4A and S14C). In addition, the Zn plating/stripping voltage profile of the cell made with the chitosan-Zn electrolyte (57% water content) shows a smaller and more stable voltage hysteresis of 116 mV (Figure 4B) than that of aqueous electrolyte (134 mV; Figure S15).

With the chitosan-Zn electrolyte, we achieved excellent cycling performance and long lifespan in symmetric Zn-metal batteries at high current densities (up to 50 mA cm^{-2}). The symmetric Zn batteries using the chitosan-Zn electrolyte can stably cycle for up to ~2,500 cycles at 5 mA cm^{-2} with capacities of 1 and 2.5 mAh cm^{-2}

Please cite this article in press as: Wu et al., A sustainable chitosan-zinc electrolyte for high-rate zinc-metal batteries, Matter (2022), https://doi.org/10.1016/j.matt.2022.07.015

(Figures S16A and S16B). At 10 mA cm^{-2}, the cell shows a polarization voltage of 100 mV and remains almost constant throughout the 1,800 cycles (red line in Figure S17A). In contrast, using the aqueous $ZnSO_4$ electrolyte, the porous chitosan-Zn electrolyte, and the densified chitosan electrolyte (without Zn^{2+} cross-linking), the cells soon failed because of either irreversible voltage increase (black line in Figure S17A) or short circuiting (Figures S17B and S17C). Furthermore, after 1,000 cycles, the symmetric Zn battery using the chitosan-Zn electrolyte showed only a slight increase of the interface resistance compared with the fresh cell (Figure S18) without short circuiting, indicating the durability of the Zn anode interface using the chitosan-Zn electrolyte. Even at a high current density of 50 mA cm^{-2}, the chitosan-Zn electrolyte can still enable stable cycling of the Zn-metal anode with a capacity of 10 mAh cm^{-2} and depth of discharge of 17.1% for 1,000 cycles without significant voltage fluctuation (Figure 4C). In contrast, using the aqueous electrolyte, the cell suffered from irreversible voltage increase and eventually failed at the 350^{th} cycle (Figure 4C).

We examined the Zn anode surface after 1,000 cycles at 10 mA cm^{-2} with the chitosan-Zn electrolyte and found that the Zn maintained platelet-like morphology (Figure S19). Such durable deposition behavior increases the Zn deposits density and reduces the surface area, suppressing interfacial side reactions for high reversibility. X-ray diffraction (XRD) patterns of the cycled Zn anodes using the chitosan-Zn and aqueous electrolytes demonstrate that $Zn_4SO_4(OH)_6 \cdot xH_2O$, which is the side product commonly found on Zn-metal anodes cycled using aqueous-based electrolytes,[37] is effectively suppressed with the chitosan-Zn electrolyte (Figure S20). The chitosan-Zn electrolyte also suppresses H_2 production, which is suggested by the reduced swelling of the coin cell cases after cycling at 50 mA cm^{-2} compared with the aqueous Zn-metal battery (Figure S21), mitigating the long-term issue of the hydrogen evolution in aqueous Zn batteries.[10]

With the chitosan-Zn electrolyte, we can cycle the Zn symmetric cell at 50 mA cm^{-2} with a cumulative plating capacity of 10 Ah cm^{-2} (Figure 4C), outperforming all previously reported symmetric cells with Zn^{2+}-conducting electrolytes (including hydrogel electrolytes and Zn salt with different additives; Table S2), demonstrating the excellent potential of the chitosan-Zn electrolyte for Zn-metal anodes. Thus, the symmetric cell built with the chitosan-Zn electrolyte shows collective advantages on current density and cumulative plated Zn capacity over other reported electrolytes (Figure 4D).

To evaluate the performance of the chitosan-Zn electrolyte in full cells, we used an organic cathode material (PBQS) to couple with the Zn-metal anode. PBQS is a promising organic electrode material for aqueous Zn batteries due to its low cost, abundant resources, high reversible capacity, and good cycling stability,[38,39] as well as its biodegradable and environmentally friendly properties as one member of quinone family.[4] Pairing the PBQS cathode (with a high PBQS mass loading of 10 mg cm^{-2}) with the Zn-metal anode and the chitosan-Zn electrolyte, the Zn full cell shows a higher discharge/charge capacity (~190 mAh g^{-1}) and lower overpotential at rate capacity of 5C (1C = 200 mA g^{-1}) than the cell using aqueous electrolyte (Figure 4E). The Zn-metal battery using the chitosan-Zn electrolyte exhibits outstanding rate performance, delivering discharge capacities of 232, 211, 186, and 156 mAh g^{-1} at 1, 2, 5, and 10C, respectively (for the 2^{nd} cycle at each rate; Figures 4F and S22A). Even at a high rate of 20C, a discharge capacity of 98 mAh g^{-1} is achieved with a good reversibility, demonstrating the high-rate capability of the full battery using the chitosan-Zn electrolyte. When the rate changes from 20

Please cite this article in press as: Wu et al., A sustainable chitosan-zinc electrolyte for high-rate zinc-metal batteries, Matter (2022), https://doi.org/10.1016/j.matt.2022.07.015

to 2C, the reversible capacity recovers to 208 mAh g^{-1}, demonstrating its excellent reversibility (Figure 4F). In addition, the cell using the chitosan-Zn electrolyte has a good capacity retention of 71% and a high Coulombic efficiency of close to 100% over 400 cycles (Figure 4G). The capacity decay is mainly due to the PBQS volume change during cycling and the induced mechanical fracture.[40] In contrast, the control cell using the aqueous electrolyte, which has a similar Zn^{2+} conductivity (99 mS cm^{-1}) to the chitosan-Zn electrolyte, only shows 157, 90, and 37 mAh g^{-1} at 5, 10, and 20C, respectively (Figures 4F and S22B). The Zn battery in the aqueous electrolyte can also deliver a discharge capacity of 206 mAh g^{-1} at 2C for 46 cycles but short circuited after the 46^{th} cycle, likely due to Zn dendrite penetration (Figure S22C). The battery using the chitosan-Zn electrolyte also achieves much better rate capacity than most Zn-metal batteries with different electrolytes,[39,41–50] which we compare by their areal capacity-current density curves (Figure S22D). Such improvements in battery performance regarding capacity, rate performance, and cycling life are attributed to the preferable Zn plating morphology and suppressed side reactions, enabled by the chitosan-Zn electrolyte.

Non-flammability and biodegradability

Aside from the high-rate and high-capacity performance, we also demonstrated the safety and sustainability of the cell using the chitosan-Zn electrolyte. As a gel electrolyte filled with aqueous solution, the chitosan-Zn electrolyte is not flammable and only shrinks and becomes soft when placed in a flame (Figures 5A–5C). We ascribe the non-flammability of the chitosan-Zn electrolyte to its non-flammable components, including the chitosan polymer[59] and aqueous electrolyte of $ZnSO_4$, which ensures the high safety of the Zn-metal batteries. Due to the utilization of biopolymeric chitosan, the chitosan-Zn electrolyte is also biodegradable, which we verified by burying the membrane in soil (Figures 5D–5F). After burying the fresh chitosan-Zn electrolyte (Figure 5D) in soil for 2 months (Figure 5E), the chitosan-Zn electrolyte became moldy (indicated by the yellow arrows in Figure 5E) and started to degrade (indicated by the white arrows in Figure 5E). It totally degraded after 5 months (Figure 5F), indicating that the chitosan-Zn electrolyte is biodegradable. The chitosan-Zn electrolyte derived from natural biomaterial (shrimp, crab, and so on) not only displays excellent performance in batteries but also releases the constitutes back to the environment in a natural way. Other components of the Zn-metal battery are either also biodegradable (PQBS cathode), environmentally friendly (aqueous solution), or recyclable (Zn-metal) (Figure 5G). Thus, the biodegradable chitosan-Zn electrolyte allows for the possibility of developing green batteries, as we schematically illustrate in Figure 5G. Moreover, due to the natural abundance of chitosan and the facile fabrication process of the chitosan-Zn electrolyte, the chitosan-Zn material is expected to have a low manufacturing cost of ~\$4.2 m^{-2} or \$46.5 kg^{-1} (see Table S3), comparable to commercial separators (e.g., Celgard).[60] Such a high-rate and high-capacity performance, as well as the high safety, biodegradability, and low cost, render chitosan-based Zn-metal batteries promising for practical large-scale energy-storage applications.

Conclusions

In conclusion, we have developed a sustainable Zn-coordinated chitosan electrolyte and demonstrate its high performance for use in Zn-metal batteries. The chitosan-Zn membrane was fabricated using a facile two-step method of Zn^{2+}-coordination of chitosan, followed by mechanical pressing, resulting in a dense structure. The chitosan-Zn membrane displays a high mechanical strength and water bonding capability, which enables a tunable Zn^{2+} conductivity and controllable Zn electrodeposition morphology. With controlled water content of 57%, the chitosan-Zn electrolyte

Please cite this article in press as: Wu et al., A sustainable chitosan-zinc electrolyte for high-rate zinc-metal batteries, Matter (2022), https://doi.org/10.1016/j.matt.2022.07.015

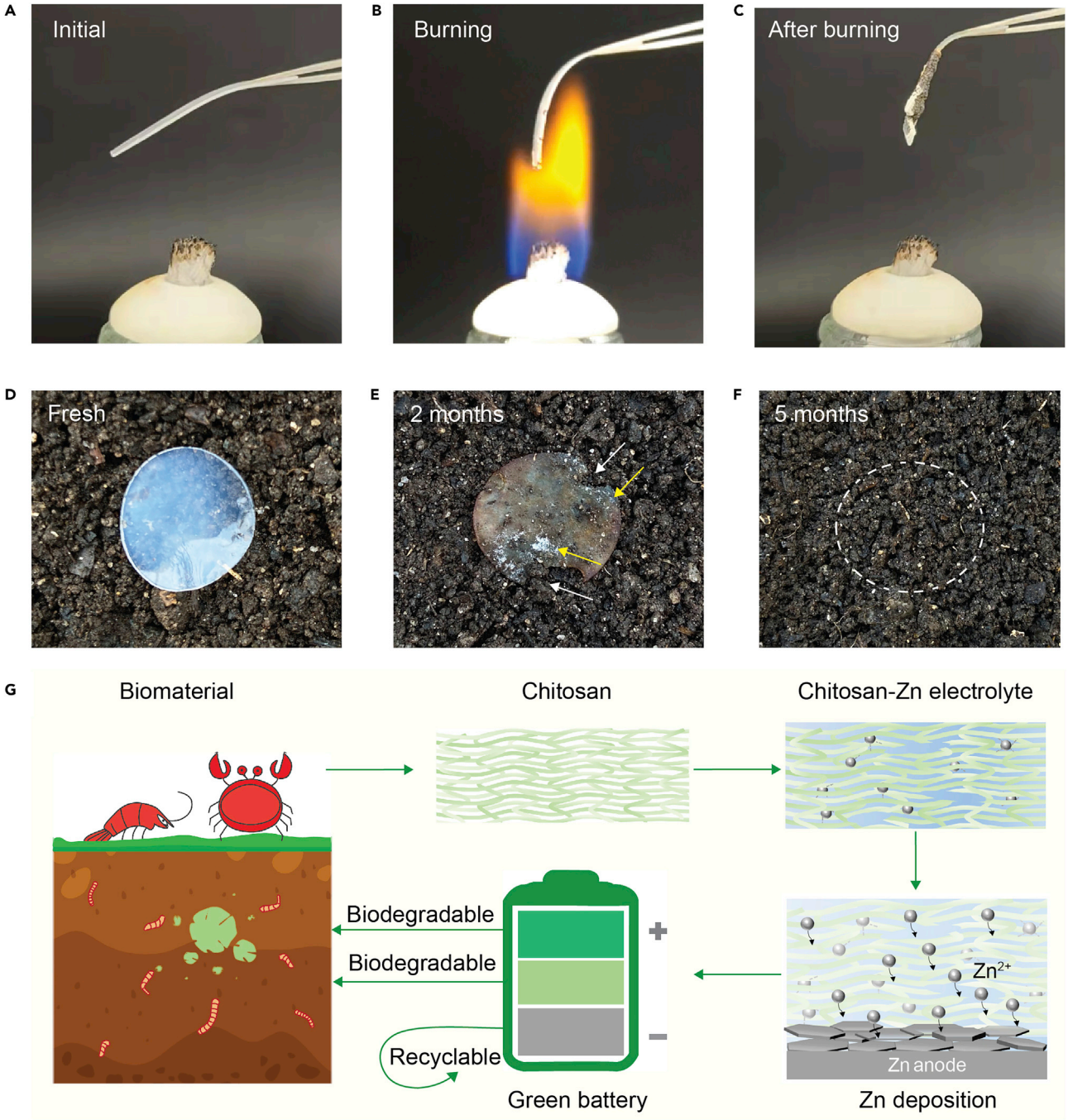

Figure 5. Safety, biodegradability, and sustainability of chitosan-Zn electrolyte

(A–C) Photos of (A) the chitosan-Zn electrolyte prior to flame exposure, (B) the chitosan-Zn electrolyte held in the flame, and (C) the chitosan-Zn electrolyte after burning.

(D–F) Photos of (D) fresh chitosan-Zn electrolyte, and chitosan-Zn electrolyte buried in soil for (E) 2 and (F) 5 months.

(G) A schematic diagram of the sustainable Zn-metal battery based on the chitosan biomaterial, which comes from the shrimps and crabs and degrades in soil after use.

exhibits a high ionic conductivity of 72 mS cm^{-1} and enables a desirable parallel Zn platelet deposition morphology. As a result, the chitosan-Zn electrolyte can enable cycle at 50 mA cm^{-2} for >1,000 cycles with excellent reversibility and high

Please cite this article in press as: Wu et al., A sustainable chitosan-zinc electrolyte for high-rate zinc-metal batteries, Matter (2022), https://doi.org/10.1016/j.matt.2022.07.015

Coulombic efficiency (99.7%). The Zn-metal full cells fabricated using the chitosan-Zn electrolyte show a high-rate performance (10–20C) and long lifespan (>400 cycles at 2C) with an areal capacity of 2.3 mAh cm^{-2} (cathode loading of 10 mg cm^{-2}), better than most of the reported Zn-metal batteries. Owing to its excellent electrochemical performance, low cost, high safety, biodegradability, and facile fabrication method, the chitosan-Zn electrolyte and its design strategy paves a way for developing high-performance and sustainable biopolymer-based electrolytes for green energy-storage and -conversion devices.

EXPERIMENTAL PROCEDURES

Resource availability

Lead contact

Further information and requests for resources should be directed to and will be fulfilled by the lead contact, Liangbing Hu (binghu@umd.edu).

Materials availability

This study did not generate new unique materials.

Data and code availability

The data presented in this work are available from the lead contact upon reasonable request.

Materials

Chitosan powder (>75% deacetylated) was purchased from Millipore Sigma. Zinc foil (100 μm in thickness) was purchased from MTI. Sodium hydroxide and zinc sulfate were purchased from Millipore Sigma and used directly without any treatment.

Preparation of the chitosan-Zn membrane

Chitosan powder (1 g) was first dissolved in 4 wt % acetic acid aqueous solution (200 mL) by stirring overnight at room temperature to produce a 0.5 wt % chitosan solution. A filtration process was used to remove the undissolved impurities. The obtained transparent chitosan solution was further concentrated through evaporation to obtain a viscous ~4 wt % chitosan solution. This chitosan solution was then drop cast on a Petri dish or cast on a PET film with a doctor blade with a solution weight of ~0.16 g cm^{-2}. The resulting chitosan wet film was then immediately immersed in a Zn^{2+}-saturated NaOH solution (0.6 wt % Zn^{2+} measured by inductively coupled plasma mass spectrometry [ICP-MS]) for 4 days, which was prepared by immersing excess Zn foil in 20 wt % NaOH solution for 1 week. A porous chitosan-Zn membrane is formed by the solvent-nonsolvent exchange process, in which the acidic aqueous solution is the solvent and the NaOH aqueous solution is the nonsolvent. The resulting porous chitosan-Zn membrane was washed with excess water. A pressure of ~5 MPa was applied to densify the porous chitosan-Zn membrane to obtain the densified chitosan-Zn membrane. The dry porous and densified chitosan-Zn membranes were freeze dried for material characterization.

Preparation of the chitosan-Zn electrolyte

The porous chitosan-Zn membrane was immersed in 2 M $ZnSO_4$ aqueous solution overnight and then pressed at 5 MPa to densify the membrane. The resulting chitosan-Zn electrolyte was then obtained after wiping excess $ZnSO_4$ solution off the surface of the densified membrane with a mass of m_0. The water content in this electrolyte is 57% based on the ratio of m_1 and m_0, where m_1 is the mass of chitosan-Zn electrolyte after removing water completely in vacuum oven at 100°C. The chitosan-Zn electrolyte samples with different water contents were prepared by

Please cite this article in press as: Wu et al., A sustainable chitosan-zinc electrolyte for high-rate zinc-metal batteries, Matter (2022), https://doi.org/10.1016/j.matt.2022.07.015

evaporating the densified membrane (m_0) in air or soaking the densified membrane in 2 M $ZnSO_4$ solution, until membranes were obtained with masses of 0.5, 0.75, 1.25, and 1.5 m_0. The calculating water content in these chitosan-Zn electrolytes is 34%, 43%, 66%, and 72%, respectively.

Battery assembly and electrochemical tests

Zn symmetric cells were assembled using Zn foils for both the cathode and anode and either the chitosan-Zn electrolyte (which also served as the separator) or aqueous electrolyte (100 μL 2 M $ZnSO_4$) with a glass-fiber separator. The asymmetric Cu||Zn cells were assembled using Cu foil and Zn foil as the cathode and anode, respectively. All cells were assembled in ambient environment using CR2032 coin cells and were tested at room temperature.

The galvanostatic plating/stripping profiles were measured at different areal capacities and different current densities on a NEWARE battery-testing system. The Zn plating/stripping Coulombic efficiencies were probed at different current densities with a charge-cutoff voltage of 1 V. EIS data were measured using a Biologic VMP3 electrochemical workstation at an amplitude of 10 mV at an open-circuit voltage.

Assembly of the Zn-PBQS battery and electrochemical tests

PBQS was synthesized following a method reported in the literature.[46] To prepare composite electrodes, PBQS, Ketjenblack (KB) carbon, and polytetrafluoroethylene (PTFE) were mixed at a mass ratio of 7:2:1 with 2 mL ethanol as the dispersant. The freestanding electrodes were cut and pressed into stainless-steel meshes (1 cm^2, 100 × 100 mesh) and dried at 80°C under vacuum for 12 h before cell assembly. The areal loading of the active material was ~10 mg cm^{-2}.

The electrochemical performances of the composite electrodes were evaluated in a split cell by using zinc foil as the anode and chitosan-Zn electrolyte (150 μm) or 80 μL of 2 M $ZnSO_4$ aqueous electrolyte with a glass-fiber separator (Whatman, 150 μm). Electrochemical characterization was performed with a potentiostat (VMP3, Biologic). The cells were tested under different charge/discharge rates of 1 to 20C, where 1C equals a current density of 200 mA g^{-1}. All electrochemical tests were run at room temperature.

Material characterization

The morphologies of the samples were studied by SEM at 10 kV on a Hitachi SU-70 with EDS analysis at 15 kV. XPS was conducted on a Thermo ESCALAB 250. The C1s peak at 284.8 eV was used as a reference to calibrate the binding energy values of other peaks. FTIR was performed with a Thermo Nicolet NEXUS 670 FTIR with an attenuated total reflectance (ATR) accessory.

XRD was performed on a Bruker D8 Advance powder diffractometer with Cu radiation (scan rate of 2° min^{-1}). N_2 adsorption/desorption isotherms were measured on a Micromeritics ASAP 2020 Porosimeter. Specific surface area and pore size were determined by the BET and Barrett-Joyner-Halenda (BJH) methods, respectively. Tensile stress-strain curves were conducted on a tabletop model testing system (Instron, Norwood, MA, USA) with a running speed of 0.1 mm min^{-1}. DSC was performed on a TA Instruments DSC Q100. The samples are first cooled to −30°C then heated to 20°C to obtain a melting curve with a cooling/heating rate of 5°C min^{-1}. ICP was conducted on a PerkinElmer NexION 300D ICP-MS, where ^{63}Cu standard solutions were used to construct a calibration curve.

SUPPLEMENTAL INFORMATION

Supplemental information can be found online at https://doi.org/10.1016/j.matt.2022.07.015.

ACKNOWLEDGMENTS

L.H. and M.W. acknowledge support from the University of Maryland A. James Clark School of Engineering and Maryland Nanocenter, its Surface Analysis Center, and AIMLab. Y.Y. acknowledges funding support from Research Corporation for Science Advancement (Scialog grant ID 27110) and Facebook Reality Labs Research. We acknowledge Dr. Jiancun Rao from the Maryland Nanocenter for his help on TEM measurements. We acknowledge Alexandra H. Brozena for help on the manuscript review.

AUTHOR CONTRIBUTIONS

Conceptualization, L.H. and M.W.; methodology, M.W. and C.Y.; investigation, M.W., Y.Z., L.X., M.H., M.C., B.C.C., S.H., and S.J.; writing – original draft, M.W. and Y.Z.; writing – review & editing, L.H.; supervision, L.H. and Y.Y.

DECLARATION OF INTERESTS

The authors declare no competing interests.

Received: April 2, 2022
Revised: June 20, 2022
Accepted: July 12, 2022
Published: September 1, 2022

REFERENCES

1. Zhang, Y., Chen, Z., Qiu, H., Yang, W., Zhao, Z., Zhao, J., and Cui, G. (2020). Pursuit of reversible Zn electrochemistry: a time-honored challenge towards low-cost and green energy storage. NPG Asia Mater. *12*, 4.
2. Yu, X., and Manthiram, A. (2021). Sustainable battery materials for next-generation electrical energy storage. Adv. Energy Sustain. Res. *2*, 2000102.
3. Chao, D., Zhou, W., Xie, F., Ye, C., Li, H., Jaroniec, M., and Qiao, S.-Z. (2020). Roadmap for advanced aqueous batteries: from design of materials to applications. Sci. Adv. *6*, 4098.
4. Xu, P., Tan, D.H., and Chen, Z. (2021). Emerging trends in sustainable battery chemistries. Trends Chem. *3*, 620–630.
5. Zhang, T., Tang, Y., Guo, S., Cao, X., Pan, A., Fang, G., Zhou, J., and Liang, S. (2020). Fundamentals and perspectives in developing zinc-ion battery electrolytes: a comprehensive review. Energy Environ. Sci. *13*, 4625–4665.
6. Blanc, L.E., Kundu, D., and Nazar, L.F. (2020). Scientific challenges for the implementation of Zn-ion batteries. Joule *4*, 771–799.
7. Hao, J., Li, X., Zhang, S., Yang, F., Zeng, X., Zhang, S., Bo, G., Wang, C., and Guo, Z. (2020). Designing dendrite-free zinc anodes for advanced aqueous zinc batteries. Adv. Funct. Mater. *30*, 2001263.
8. Kang, L., Cui, M., Jiang, F., Gao, Y., Luo, H., Liu, J., Liang, W., and Zhi, C. (2018). Nanoporous $CaCO_3$ coatings enabled uniform Zn stripping/plating for long-life zinc rechargeable aqueous batteries. Adv. Energy Mater. *8*, 1801090.
9. Huang, S., Zhu, J., Tian, J., and Niu, Z. (2019). Recent progress in the electrolytes of aqueous zinc-ion batteries. Chem. Eur. J. *25*, 14480–14494.
10. Verma, V., Kumar, S., Manalastas, W., and Srinivasan, M. (2021). Undesired reactions in aqueous rechargeable zinc ion batteries. ACS Energy Lett. *6*, 1773–1785.
11. Wan, F., Zhou, X., Lu, Y., Niu, Z., and Chen, J. (2020). Energy storage chemistry in aqueous zinc metal batteries. ACS Energy Lett. *5*, 3569–3590.
12. Qiu, H., Du, X., Zhao, J., Wang, Y., Ju, J., Chen, Z., Hu, Z., Yan, D., Zhou, X., and Cui, G. (2019). Zinc anode-compatible in-situ solid electrolyte interphase via cation solvation modulation. Nat. Commun. *10*, 5374.
13. Zhang, Y., Yang, G., Lehmann, M.L., Wu, C., Zhao, L., Saito, T., Liang, Y., Nanda, J., and Yao, Y. (2021). Separator effect on zinc electrodeposition behavior and its implication for zinc battery lifetime. Nano Lett. *21*, 10446–10452.
14. Yang, H., Chang, Z., Qiao, Y., Deng, H., Mu, X., He, P., and Zhou, H. (2020). Constructing a Super-saturated electrolyte front surface for stable rechargeable aqueous zinc batteries. Angew. Chem. Int. Ed. Engl. *59*, 9377–9381.
15. Wang, F., Borodin, O., Gao, T., Fan, X., Sun, W., Han, F., Faraone, A., Dura, J.A., Xu, K., and Wang, C. (2018). Highly reversible zinc metal anode for aqueous batteries. Nat. Mater. *17*, 543–549.
16. Chen, C., Matsumoto, K., Kubota, K., Hagiwara, R., and Xu, Q. (2019). A room-temperature molten hydrate electrolyte for rechargeable zinc–air batteries. Adv. Energy Mater. *9*, 1970086.
17. Naveed, A., Yang, H., Yang, J., Nuli, Y., and Wang, J. (2019). Highly reversible and rechargeable safe Zn batteries based on a triethyl phosphate electrolyte. Angew. Chem. Int. Ed. Engl. *58*, 2760–2764.
18. Wang, N., Yang, Y., Qiu, X., Dong, X., Wang, Y., and Xia, Y. (2020). Stabilized rechargeable aqueous zinc batteries using ethylene glycol as water blocker. ChemSusChem *13*, 5556–5564.
19. Li, H., Han, C., Huang, Y., Huang, Y., Zhu, M., Pei, Z., Xue, Q., Wang, Z., Liu, Z., Tang, Z., et al. (2018). An extremely safe and wearable solid-state zinc ion battery based on a hierarchical structured polymer electrolyte. Energy Environ. Sci. *11*, 941–951.
20. Han, D., Cui, C., Zhang, K., Wang, Z., Gao, J., Guo, Y., Zhang, Z., Wu, S., Yin, L., Weng, Z., et al. (2021). A non-flammable hydrous organic electrolyte for sustainable zinc batteries. Nat. Sustain. *5*, 205–213.

21. Cao, Z., Zhuang, P., Zhang, X., Ye, M., Shen, J., and Ajayan, P.M. (2020). Strategies for dendrite-free anode in aqueous rechargeable zinc ion batteries. Adv. Energy Mater. *10*, 2001599.

22. Wang, D., Li, H., Liu, Z., Tang, Z., Liang, G., Mo, F., Yang, Q., Ma, L., and Zhi, C. (2018). A nanofibrillated cellulose/polyacrylamide electrolyte-based flexible and sewable high-performance Zn–MnO_2 battery with superior shear resistance. Small *14*, 1803978.

23. Yang, L., Song, L., Feng, Y., Cao, M., Zhang, P., Zhang, X.-F., and Yao, J. (2020). Zinc ion trapping in a cellulose hydrogel as a solid electrolyte for a safe and flexible supercapacitor. J. Mater. Chem. *8*, 12314–12318.

24. Lizundia, E., and Kundu, D. (2021). Advances in natural biopolymer-based electrolytes and separators for battery applications. Adv. Funct. Mater. *31*, 2005646.

25. Tang, B., Shan, L., Liang, S., and Zhou, J. (2019). Issues and opportunities facing aqueous zinc-ion batteries. Energy Environ. Sci. *12*, 3288–3304.

26. Peter, S., Lyczko, N., Gopakumar, D., Maria, H.J., Nzihou, A., and Thomas, S. (2020). Chitin and chitosan based composites for energy and environmental applications: a review. Waste Biomass Valorization *12*, 4777–4804.

27. Yoo, S., Kim, J.-H., Shin, M., Park, H., Kim, J.-H., Lee, S.-Y., and Park, S. (2015). Hierarchical multiscale hyperporous block copolymer membranes via tunable dual-phase separation. Sci. Adv. *1*, e1500101.

28. Ma, C., Li, F., Wang, C., He, M., Shen, C., Sand, W., and Liu, Y. (2018). Tuning the adsorption behaviour of β-structure chitosan by metal binding. Environ. Chem. *15*, 267–277.

29. Zhu, Y.S., Xiao, S.Y., Li, M.X., Chang, Z., Wang, F.X., Gao, J., and Wu, Y.P. (2015). Natural macromolecule based carboxymethyl cellulose as a gel polymer electrolyte with adjustable porosity for lithium ion batteries. J. Power Sources *288*, 368–375.

30. Chen, M., Chen, J., Zhou, W., Xu, J., and Wong, C.-P. (2019). High-performance flexible and self-healable quasi-solid-state zinc-ion hybrid supercapacitor based on borax-crosslinked polyvinyl alcohol/nanocellulose hydrogel electrolyte. J. Mater. Chem. *7*, 26524–26532.

31. Dai, L., Arcelus, O., Sun, L., Wang, H., Carrasco, J., Zhang, H., Zhang, W., and Tang, J. (2019). Embedded 3D Li^+ channels in a water-in-salt electrolyte to develop flexible supercapacitors and lithium-ion batteries. J. Mater. Chem. *7*, 24800–24806.

32. Li, H., Liu, Z., Liang, G., Huang, Y., Huang, Y., Zhu, M., Pei, Z., Xue, Q., Tang, Z., Wang, Y., et al. (2018). Waterproof and tailorable elastic rechargeable yarn zinc ion batteries by a cross-linked polyacrylamide electrolyte. ACS Nano *12*, 3140–3148.

33. Rana, H.H., Park, J.H., Gund, G.S., and Park, H.S. (2020). Highly conducting, extremely durable, phosphorylated cellulose-based ionogels for renewable flexible supercapacitors. Energy Storage Mater. *25*, 70–75.

34. Zheng, J., and Archer, L.A. (2021). Controlling electrochemical growth of metallic zinc electrodes: toward affordable rechargeable energy storage systems. Sci. Adv. *7*, eabe0219.

35. Hagopian, A., Doublet, M.-L., and Filhol, J.-S. (2020). Thermodynamic origin of dendrite growth in metal anode batteries. Energy Environ. Sci. *13*, 5186–5197.

36. Yao, Y., Wang, Z., Li, Z., and Lu, Y.-C. (2021). A dendrite-free Tin anode for high-energy aqueous redox flow batteries. Adv. Mater. *33*, 2008095.

37. Yang, Q., Li, Q., Liu, Z., Wang, D., Guo, Y., Li, X., Tang, Y., Li, H., Dong, B., and Zhi, C. (2020). Dendrites in Zn-based batteries. Adv. Mater. *32*, 2001854.

38. Liang, Y., Jing, Y., Gheytani, S., Lee, K.-Y., Liu, P., Facchetti, A., and Yao, Y. (2017). Universal quinone electrodes for long cycle life aqueous rechargeable batteries. Nat. Mater. *16*, 841–848.

39. Zhao, Q., Huang, W., Luo, Z., Liu, L., Lu, Y., Li, Y., Li, L., Hu, J., Ma, H., and Chen, J. (2018). High-capacity aqueous zinc batteries using sustainable quinone electrodes. Sci. Adv. *4*, 1761.

40. Zhang, Y., Zhao, L., Liang, Y., Wang, X., and Yao, Y. (2022). Effect of electrolyte anions on the cycle life of a polymer electrode in aqueous batteries. eScience *2*, 110–115.

41. Dawut, G., Lu, Y., Miao, L., and Chen, J. (2018). High-performance rechargeable aqueous Zn-ion batteries with a poly(benzoquinonyl sulfide) cathode. Inorg. Chem. Front. *5*, 1391–1396.

42. Zhang, N., Cheng, F., Liu, J., Wang, L., Long, X., Liu, X., Li, F., and Chen, J. (2017). Rechargeable aqueous zinc-manganese dioxide batteries with high energy and power densities. Nat. Commun. *8*, 405.

43. Guo, Z., Ma, Y., Dong, X., Huang, J., Wang, Y., and Xia, Y. (2018). An environmentally friendly and flexible aqueous zinc battery using an organic cathode. Angew. Chem. Int. Ed. Engl. *57*, 11737–11741.

44. Xiong, T., Yu, Z.G., Wu, H., Du, Y., Xie, Q., Chen, J., Zhang, Y., Pennycook, S.J., Lee, W.S.V., and Xue, J. (2019). Defect engineering of oxygen-deficient manganese oxide to achieve high-performing aqueous zinc ion battery. Adv. Energy Mater. *9*, 1803815.

45. Jiao, T., Yang, Q., Wu, S., Wang, Z., Chen, D., Shen, D., Liu, B., Cheng, J., Li, H., Ma, L., et al. (2019). Binder-free hierarchical VS_2 electrodes for high-performance aqueous Zn ion batteries towards commercial level mass loading. J. Mater. Chem. *7*, 16330–16338.

46. Song, Z., Qian, Y., Zhang, T., Otani, M., and Zhou, H. (2015). Poly(benzoquinonyl sulfide) as a high-energy organic cathode for rechargeable Li and Na batteries. Adv. Sci. *2*, 1500124.

47. Tang, F., Zhou, W., Chen, M., Chen, J., and Xu, J. (2019). Flexible free-standing paper electrodes based on reduced graphene oxide/δ-$Na_xV_2O_5{\cdot}nH_2O$ nanocomposite for high-performance aqueous zinc-ion batteries. Electrochim. Acta. *328*, 135137.

48. Ma, H., Tian, X., Wang, T., Tang, K., Liu, Z., Hou, S., Jin, H., and Cao, G. (2021). Tailoring pore structures of 3D printed cellular high-loading cathodes for advanced rechargeable zinc-ion batteries. Small *17*, 2100746.

49. Liu, P., Liu, W., Huang, Y., Li, P., Yan, J., and Liu, K. (2020). Mesoporous hollow carbon spheres boosted, integrated high performance aqueous Zn-Ion energy storage. Energy Storage Mater. *25*, 858–865.

50. Leng, K., Li, G., Guo, J., Zhang, X., Wang, A., Liu, X., and Luo, J. (2020). A safe polyzwitterionic hydrogel electrolyte for long-life quasi-solid state zinc metal batteries. Adv. Funct. Mater. *30*, 2001317.

51. Zhu, M., Wang, X., Tang, H., Wang, J., Hao, Q., Liu, L., Li, Y., Zhang, K., and Schmidt, O.G. (2020). Antifreezing hydrogel with high zinc reversibility for flexible and durable aqueous batteries by cooperative hydrated cations. Adv. Funct. Mater. *30*, 1907218.

52. Liang, P., Yi, J., Liu, X., Wu, K., Wang, Z., Cui, J., Liu, Y., Wang, Y., Xia, Y., and Zhang, J. (2020). Highly reversible Zn anode enabled by controllable formation of nucleation sites for Zn-based batteries. Adv. Funct. Mater. *30*, 1908528.

53. Hou, Z., Tan, H., Gao, Y., Li, M., Lu, Z., and Zhang, B. (2020). Tailoring desolvation kinetics enables stable zinc metal anodes. J. Mater. Chem. *8*, 19367–19374.

54. Xu, W., Zhao, K., Huo, W., Wang, Y., Yao, G., Gu, X., Cheng, H., Mai, L., Hu, C., and Wang, X. (2019). Diethyl ether as self-healing electrolyte additive enabled long-life rechargeable aqueous zinc ion batteries. Nano Energy *62*, 275–281.

55. Ma, L., Chen, S., Li, N., Liu, Z., Tang, Z., Zapien, J.A., Chen, S., Fan, J., and Zhi, C. (2020). Hydrogen-free and dendrite-free all-solid-state Zn-ion batteries. Adv. Mater. *32*, 1908121.

56. Yin, Y., Wang, S., Zhang, Q., Song, Y., Chang, N., Pan, Y., Zhang, H., and Li, X. (2020). Dendrite-free zinc deposition induced by Tin-modified multifunctional 3D host for stable zinc-based flow battery. Adv. Mater. *32*, 1906803.

57. Zhao, J., Zhang, J., Yang, W., Chen, B., Zhao, Z., Qiu, H., Dong, S., Zhou, X., Cui, G., and Chen, L. (2019). Water-in-deep eutectic solvent" electrolytes enable zinc metal anodes for rechargeable aqueous batteries. Nano Energy *57*, 625–634.

58. Shinde, S.S., Jung, J.Y., Wagh, N.K., Lee, C.H., Kim, D.-H., Kim, S.-H., Lee, S.U., and Lee, J.-H. (2021). Ampere-hour-scale zinc–air pouch cells. Nat. Energy *6*, 592–604.

59. Xiao, Y., Zheng, Y., Wang, X., Chen, Z., and Xu, Z. (2014). Preparation of a chitosan-based flame-retardant synergist and its application in flame-retardant polypropylene. J. Appl. Polym. Sci. *131*, 40845.

60. Schmuch, R., Wagner, R., Hörpel, G., Placke, T., and Winter, M. (2018). Performance and cost of materials for lithium-based rechargeable automotive batteries. Nat. Energy *3*, 267–278.